
High Order Finite Difference Schemes for the Transparent Boundary Conditions and Their Applications in the 1D Schrödinger-Poisson Problem

Meili Guo · Haiyan Jiang · Tiao Lu · Wenqi Yao*

Abstract The 1D Schrödinger equation closed with the transparent boundary conditions (TBCs) is known as a successful model for describing quantum effects, and is usually considered with a self-consistent Poisson equation in simulating quantum devices. We introduce discrete fourth order transparent boundary conditions (D4TBCs), which have been proven to be essentially non-oscillating when the potential vanishes, and to share the same accuracy order with the finite difference scheme used to discretize the 1D Schrödinger equation. Furthermore, a framework of analytic discretization of TBCs (aDTBCs) is proposed, which does not introduce any discretization error, thus is accurate. With the accurate discretizations, one is able to improve the accuracy of the discretization for the 1D Schrödinger problem to arbitrarily high levels. As numerical tools, two globally fourth order compact finite difference schemes are proposed for the 1D Schrödinger-Poisson problem, involving either of the D4TBCs or the aDTBCs, respectively, and the uniqueness of solutions of both discrete Schrödinger problems are rigorously proved. Numerical experiments, including simulations of a resistor and two nanoscale resonant tunneling diodes, verify the accuracy order of the discretization schemes and show potential of the numerical algorithm introduced for the 1D Schrödinger-Poisson problem in simulating various quantum devices.

*Corresponding author

Meili Guo
School of Mathematics and Statistics, Beijing Institute of Technology, 100081, Beijing, China
E-mail: guomeili@bit.edu.cn

Haiyan Jiang
School of Mathematics and Statistics, Beijing Institute of Technology, 100081, Beijing, China
E-mail: hyjiang@bit.edu.cn

Tiao Lu
HEDPS, CAPT, LMAM, School of Mathematical Sciences, Peking University, 100871, Beijing, China
E-mail: tlu@pku.edu.cn

Wenqi Yao
School of Mathematics, South China University of Technology, 510641, Guangzhou, Guangdong, China
E-mail: yaowq@scut.edu.cn

Keywords 1D Schrödinger-Poisson problem · Transparent boundary condition · Compact finite difference scheme · Discrete transparent boundary condition · Resonant tunneling diode

Mathematics Subject Classification (2020) 34L40 · 65L10 · 65L20

1 Introduction

The present trend of semiconductor fabrication technology shows a dramatic size reduction of semiconductor devices. As a result, quantum transport models are considered in order to clearly understand the electrical properties of nanoscale devices. Three equivalent approaches are proposed to model nanoscale devices, including the Wigner transport equation[8, 7], the non-equilibrium Green's function(NEGF) method [5, 9], and the Schrödinger equation[17, 16, 14].

We use the 1D Schrödinger equation to describe the characteristics of quantum devices, where appropriate boundary conditions are needed to confine the problem in a bounded domain. The set of transparent boundary conditions (TBCs)[2] is a good candidate, and the yielded 1D Schrödinger problem, i.e., the 1D Schrödinger equation equipped with the TBCs, admits a unique solution, thus is well-defined. When simulating realistic devices, one has to consider self-consistent potential due to the difference of electron density and doping density. Therefore, a nonlinear 1D Schrödinger-Poisson problem is yielded naturally, by taking into account a potential governed by a Poisson equation equipped with appropriate boundary conditions, such as the electric neutrality boundary conditions used in this paper.

Discretizing TBCs is crucial in the development of numerical tools for solving the 1D Schrödinger problem. As is described in [1], inappropriate discretizations of TBCs lead to unphysical spurious oscillations in numerical solutions when potential vanishes. To solve this problem, a set of discrete fourth order transparent boundary conditions(D4TBCs) are introduced in this paper together with a fourth order compact finite difference discretization of the 1D Schrödinger equation. In addition, we prove the solution of the yielded discretization system corresponding to the 1D Schrödinger problem is unique with the form of discrete plain waves, which in turn explains extinction of spurious oscillations when potential vanishes. However, discrete transparent boundary conditions(DTBCs), no matter our D4TBCs or Arnold's[1], have drawbacks. To deduce discrete transparent boundary conditions, a discrete dispersion relation is needed, to obtain which an algebraic equation has to be solved. The order of the algebraic equation is determined by the stencil used for spatial discretization of the 1D Schrödinger equation, and the larger the stencil is, the higher the order of the algebraic equation will be. Furthermore, DTBCs introduce discretization error. To overcome drawbacks possessed by DTBCs, we further propose the framework of analytic discrete transparent boundary conditions(aDTBCs), which is accurate in discretizing the TBCs. More importantly, without high order algebraic equations to solve, we are able to improve the accuracy order of the discretization of the 1D Schrödinger problem to arbitrarily high, by using aDTBCs. For numerical simulations, we introduce a fourth order compact finite difference discretization of

the 1D Schrödinger problem involving the aDTBCs, which also well-defined due to the uniqueness of solution.

The resonant tunneling diode (RTD) has been widely used as a high-frequency and low-consumption oscillator or switch, and is studied both experimentally and theoretically over decades [6, 3]. In order to simulate RTDs, we propose an algorithm to solve the 1D Schrödinger-Poisson problem, where two discrete models are available, by equipping D4TBCs and aDTBCs, respectively. Numerical experiments are carried out following the algorithm and include two stages. In the first stage, we simulate a classic $n^{++} - n^+ - n^{++}$ resistor and an RTD, with the potential known as *a priori*, to verify fourth order accuracy of both discrete models. In the second stage, the algorithm is applied to simulate another RTD, with the potential updated simultaneously. I-V characteristic curves of both RTDs are simulated, where typical features of RTDs are observed, including negative differential resistance [19, 18], and corresponding performance in electron density, potential and transmission coefficients.

This article is organized as follows. In Sect. 2, we make a brief review about the 1D Schrödinger-Poisson problem. Finite difference discretizations of the Schrödinger equation and TBCs are thoroughly discussed in Sect. 3, where well-posedness and accuracy of yielded discrete systems are proved. Discretization of the self-consistent Poisson equation equipped with electric neutrality boundary conditions is given in Sect. 4, and an algorithm for solving the discrete Schrödinger-Poisson problem is introduced subsequently. Sect. 5 is devoted to simulations of a short $n^{++} - n^+ - n^{++}$ resistor and two resonant tunneling diodes by using the algorithm presented in Sect. 4.

2 1D Schrödinger-Poisson problem

We consider 1D Schrödinger equation on the real line:

$$\left(-\frac{\hbar^2}{2m^*} \frac{d^2}{dx^2} + V(x)\right) \psi(x; k) = E \psi(x; k), \quad x \in \mathbb{R}, \quad \forall k \in \mathbb{R}, \quad (1)$$

where $\psi(x; k)$ denotes the complex wave function of the electron, $E = \frac{\hbar^2 k^2}{2m^*}$ is the energy of an electron at steady state, physical parameters \hbar and m^* are the reduced Planck constant and the effective mass of the electron. The potential function $V(x) = V_b(x) + V_s(x)$, where $V_b(x)$ is the conduction band structure, and $V_s(x)$ is an external potential exerted to the device. $V_s(x)$ is either a given potential function or determined by a Poisson equation equipped with Neumann boundary conditions, which reads

$$-\frac{d^2}{dx^2} V_s(x) = \frac{q_e^2}{\varepsilon} (n(x) - N_d(x)), \quad x \in [0, L], \quad (2)$$

$$V_s'(0) = 0, \quad V_s'(L) = 0, \quad (3)$$

where ε is the dielectric constant, q_e is the electronic charge, $n(x)$ and $N_d(x)$ denote electron density and doping density, respectively. Furthermore, V is extended to $x < 0$ and $x > L$ by setting

$$V(x) = \begin{cases} V(0), & x < 0, \\ V(L), & x > L, \end{cases} \quad (4)$$

in order to meet the requirement of (1). When (4) is applied, (1) admits solution which takes the form of:

$$\psi(x; k) = \begin{cases} Ae^{-ik_1x} + Be^{ik_1x}, & x \leq 0, \\ Ce^{-ik_2x} + De^{ik_2x}, & x \geq L, \end{cases} \quad (5)$$

where A, B, C and D are arbitrary constants, and $k_1 = \sqrt{\frac{2m^*(E-V(0))}{\hbar^2}}$, $k_2 = \sqrt{\frac{2m^*(E-V(L))}{\hbar^2}}$, where $E \geq \max\{V(0), V(L)\}$ is mandatory. Let the wave $\psi(x; k)$ enter the device region, i.e., $x \in [0, L]$, from $x \leq 0$ with amplitude 1, and let a part of the wave be reflected at $x = 0$ while the remaining part be transmitted and travel to $+\infty$. Based on the above assumption, (5) is further rewritten as

$$\psi(x; k) = \begin{cases} re^{-ik_1x} + e^{ik_1x}, & x \leq 0, \\ te^{ik_2x}, & x \geq L, \end{cases} \quad (6)$$

where r and t are the so called reflection and transmission coefficients satisfying $|r|^2 + |t|^2 = 1$. (1) and (2) would not form a well-posed problem confined to $x \in [0, L]$, unless appropriate boundary conditions are equipped to (1) restricted on $x \in [0, L]$. As discussed in [2], artificial transparent boundary conditions(TBCs) are appended to close (1), which read

$$\psi'(0; k) + ik_1\psi(0; k) = 2ik_1, \quad (7)$$

$$\psi'(L; k) - ik_2\psi(L; k) = 0. \quad (8)$$

One thing is noticed that TBCs are necessary conditions of (6), without requiring the *priori* values of R and T . At equilibrium, the device is connected to two contacts with the same Fermi levels, and the electron density $n(x)$ in (2) is related to the wave function through

$$n(x) = \frac{1}{2\pi} \int_{-\infty}^{\infty} F(E_F - E(k)) |\psi(x; k)|^2 dk, \quad (9)$$

where

$$F(E_F - E) = \frac{m^*k_B T_L}{\pi\hbar^2} \ln \left(1 + \exp \left(\frac{E_F - E}{k_B T_L} \right) \right), \quad (10)$$

and E_F denotes the Fermi level of the left contact, k_B and T_L are Boltzmann constant and temperature of lattice, respectively. However, when a bias voltage V_{ds} is applied to one of two contacts, saying the right one, then the total electron density is given by[4]

$$n(x) = \frac{1}{2\pi} \left[\int_0^{\infty} F(E_F - E(k)) |\psi(x; k)|^2 dk + \int_{-\infty}^0 F(E_F - q_e V_{ds} - E(k)) |\psi(x; k)|^2 dk \right]. \quad (11)$$

Under this circumstance, the current density reads

$$I = \frac{q_e}{2\pi\hbar} \int_0^{\infty} T(E) [F(E_F - E) - F(E_F - q_e V_{ds} - E)] dE, \quad (12)$$

where the transmission coefficient $T(E)$ is defined as the ratio of the transmitted current I_{trans} and the incident current I_{inc} , and can be expressed as

$$T(E) = \frac{I_{\text{trans}}}{I_{\text{inc}}} = 1 - |r|^2. \quad (13)$$

3 Discretization schemes for the 1D Schrödinger problem

The whole problem contains two subproblems, i.e., the 1D Schrödinger problem((1) equipped with TBCs), and the self-consistent Poisson problem((2)-(3)), and they both correspond to one model problem:

$$u_{xx} = f(x), \quad x \in [0, L], \quad (14)$$

$$u_x(0) + a_l u(0) = b_l, \quad (15)$$

$$u_x(L) + a_r u(L) = b_r, \quad (16)$$

where $u, f, a_{l,r}, b_{l,r} \in \mathbb{C}$ depend on the specific problem. In this section, we firstly propose a globally fourth order compact scheme for solving the model problem (14), which could be directly applied to discretize the Schrödinger equation and the Poisson equation. In the rest of this section, lots of efforts are devoted to propose and discuss two optimal discretizations of the TBCs, i.e., the D4TBCs and the aDTBCs.

3.1 A globally fourth order compact scheme for the model problem

Set a uniform mesh, saying $x_i = i\Delta x$, $i = 0, 1, \dots, N_x$, $N_x = \frac{L}{\Delta x}$. Following one of the traditional ways of constructing compact finite difference schemes[11, 12], we approximate the first and second derivatives of any smooth function $u(x)$ via the linear combination of nodal values:

$$\sum_{k=-p}^p a_k (u_x)_{j+k} = \frac{1}{\Delta x} \sum_{k=1}^q b_k (u_{j+k} - u_{j-k}), \quad (17)$$

$$\sum_{k=-l}^l \alpha_k (u_{xx})_{j+k} = \frac{1}{\Delta x^2} \sum_{k=1}^s \beta_k (u_{j+k} - 2u_j + u_{j-k}), \quad (18)$$

where u_i , $(u_x)_i$ and $(u_{xx})_i$ represent approximations of u , u_x and u_{xx} at x_i , respectively. Let $p = q = l = s = 1$ and match Taylor series coefficients of both sides of (17) and (18) at x_i to fourth order, respectively. As a result, one gets fourth order compact schemes for discretizing u_x and u_{xx} at x_i , $i = 1, 2, \dots, N_x - 1$, which read

$$\frac{1}{4} (u_x)_{i-1} + (u_x)_i + \frac{1}{4} (u_x)_{i+1} = \frac{3}{4\Delta x} (u_{i+1} - u_{i-1}), \quad (19)$$

and

$$\frac{1}{10} (u_{xx})_{i-1} + (u_{xx})_i + \frac{1}{10} (u_{xx})_{i+1} = \frac{6}{5\Delta x^2} (u_{i+1} - 2u_i + u_{i-1}). \quad (20)$$

Recalling that u solves (14), we replace $(u_{xx})_{i\pm 1}$ (20) with $f_{i\pm 1}$, where f_i represents the approximation of $f(x_i)$ (with at least fourth order accuracy), and obtain a fourth order discretization scheme for (14), which reads

$$\left(\lambda u_{j-1} - f_{j-1}\right) - \left(2\lambda u_j + 10f_j\right) + \left(\lambda u_{j+1} - f_{j+1}\right) = 0, \quad j = 1 \cdots, N_x - 1, \quad (21)$$

where $\lambda = \frac{12}{\Delta x^2}$. To discretize (15)-(16), two ghost points: $x_{-1} \triangleq x_0 - \Delta x$ and $x_{N_x+1} \triangleq x_{N_x} + \Delta x$ are introduced. We further adopt Taylor series expansion of $u_x(x_{i-1})$ and $u_x(x_{i+1})$ at x_i up to fourth order in (19), and obtain

$$\frac{3}{2}(u_x)_i + \frac{\Delta x^2}{4}(u_{xxx})_i = \frac{3}{2}(u_x)_i + \frac{\Delta x^2}{4}(f_x)_i = \frac{3}{4\Delta x}(u_{i+1} - u_{i-1}), \quad (22)$$

where (14) is used. Therefore, we use second order central finite difference scheme to replace $(f_x)_i$ in (22) and obtain an alternative fourth order discretization of $u_x(x_i)$, which reads

$$(u_x)_i = -\frac{\Delta x}{12}(f_{i+1} - f_{i-1}) + \frac{1}{2\Delta x}(u_{i+1} - u_{i-1}). \quad (23)$$

We will discuss the usage of (23) in discretizing boundary conditions of Schrödinger equation and Poisson equation in detail, respectively, in subsequent sections.

3.2 The D4TBCs

We instantiate (14) with the Schrödinger problem. Applying (21), we discretize (1) at interior grid nodes as

$$\left(\lambda \psi_{j-1} - f_{j-1}\right) - \left(2\lambda \psi_j + 10f_j\right) + \left(\lambda \psi_{j+1} - f_{j+1}\right) = 0, \quad j = 1, 2 \cdots, N_x - 1. \quad (24)$$

where $f_j = \frac{2m^*}{\hbar^2}(V_j - E)\psi_j$, V_j and ψ_j denote by the approximations of $V(x_j)$ and $\psi(x_j; k)$, respectively. Furthermore, $\psi_x(0; k)$ is approximated with $(\psi_x)_0$, where

$$(\psi_x)_0 = \left[\frac{1}{2\Delta x} - \frac{\Delta x}{12} \frac{2m^*}{\hbar^2}(V_1 - E) \right] \psi_1 - \left[\frac{1}{2\Delta x} - \frac{\Delta x}{12} \frac{2m^*}{\hbar^2}(V_0 - E) \right] \psi_{-1}, \quad (25)$$

by setting $i = 0$ in (23), replacing $f_{\pm 1}$ with $\frac{2m^*}{\hbar^2}(V_{\pm 1} - E)\psi_{\pm 1}$, where $V_{-1} = V_0$ according to (4). Similarly, one obtains

$$(\psi_x)_{N_x} = \left[\frac{1}{2\Delta x} - \frac{\Delta x}{12} \frac{2m^*}{\hbar^2}(V_{N_x} - E) \right] \psi_{N_x+1} - \left[\frac{1}{2\Delta x} - \frac{\Delta x}{12} \frac{2m^*}{\hbar^2}(V_{N_x-1} - E) \right] \psi_{N_x-1}. \quad (26)$$

Substituting (25) and (26) in (7) and (8), and combining (24) at boundary grid points x_0 and x_{N_x} to eliminate ψ_{-1} and ψ_{N_x+1} , respectively, one obtains discretizations of (7) and (8) respectively as

$$a_0\psi_0 + b_1\psi_1 = d_0, \quad (27)$$

and

$$b_{N_x-1}\psi_{N_x-1} + a_{N_x}\psi_{N_x} = 0, \quad (28)$$

where

$$\begin{aligned}
a_0 &= -2t + 10(E - V_0) + 2ik_1t\Delta x \frac{t + E - V_0}{t + 2(E - V_0)}, \\
b_1 &= t + E - V_1 + (t + 2(E - V_1)) \frac{t + E - V_0}{t + 2(E - V_0)}, \\
d_0 &= 4ik_1t\Delta x \frac{t + E - V_0}{t + 2(E - V_0)}, \\
b_{N_x-1} &= t + E - V_{N_x-1} + (t + 2(E - V_{N_x-1})) \frac{t + E - V_{N_x}}{t + 2(E - V_{N_x})}, \\
a_{N_x} &= -2t + 10(E - V_{N_x}) + 2ik_2t\Delta x \frac{t + E - V_{N_x}}{t + 2(E - V_{N_x})},
\end{aligned}$$

with $t = \frac{\hbar^2}{2m^*} \lambda$. From now on, we shall call (27) + (28) the compact fourth order transparent boundary conditions (C4TBCs). Consequently, a globally fourth order compact discretization scheme is yielded for the Schrödinger problem, i.e., (24) equipped with the C4TBCs.

Although (24) equipped with the C4TBCs possesses a desirable accuracy order in discretizing the Schrödinger problem, it introduces spurious oscillation in numerical solution when $V(x)$ vanishes. We illustrate this phenomenon through an example. Let $V(x) \equiv 0$, $E = 0.5$, $L = 10$, and a wave enter from $x = 0$. Parameters $\hbar = m^* = 1$ for simplicity. Because $V \equiv 0$, the wave is completely transmitted through $x = L$, thus $\psi^*(x) = e^{ikx}$ solves the Schrödinger problem with $k = \sqrt{\frac{2m^*E}{\hbar^2}}$. Norm of numerical wave functions of the Schrödinger problem solved with different schemes are collected in **Fig. 1**. Result corresponding to (24) equipped with the C4TBCs, is plotted in red dash line. Corresponding curve of the exact wave function, i.e., $\psi^*(x) = e^{ikx}$, is also shown in blue solid line as reference. Obviously, spurious oscillation occurs when (24) is equipped with the C4TBCs.

Recalling (6), one notices it is insufficient to only consider high order discretizations of the TBCs, however the discrete form of the real solution is the priority. Based on the work originally introduced in [1], we assume discrete wave solutions for $x \leq 0$ and $x \geq L$:

$$\psi_j = \begin{cases} \alpha^j, & j \leq 0, \\ \beta^j, & j \geq N_x. \end{cases} \quad (29)$$

Substituting (29) in (24), and letting $V(x)$ vanishes for $x \notin (0, L)$, one obtains two distinct values of α :

$$\alpha_{\pm} = \frac{t - 5(E - V_0) \pm i\sqrt{12(E - V_0)(t - 2(E - V_0))}}{t + (E - V_0)},$$

and two distinct values of β :

$$\beta_{\pm} = \frac{t - 5(E - V_{N_x}) \pm i\sqrt{12(E - V_{N_x})(t - 2(E - V_{N_x}))}}{t + (E - V_{N_x})}.$$

Therefore, when $t > \max\{2(E - V_0), 2(E - V_{N_x})\}$, $|\alpha_{\pm}| = |\beta_{\pm}| = 1$ due to

$$\alpha_{\pm} = e^{\pm ik_1 \Delta x}, \beta_{\pm} = e^{\pm ik_2 \Delta x}, \quad (30)$$

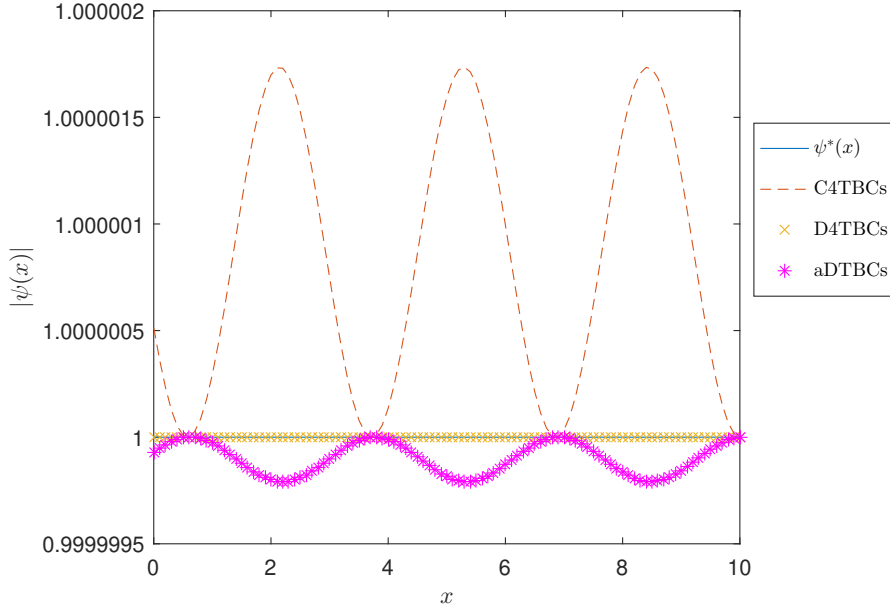


Fig. 1 Norm of numerical wave functions of the Schrödinger problem, where different discrete boundary conditions are compared

with \tilde{k}_1 and \tilde{k}_2 the approximations of k_1 and k_2 , respectively. The so called discrete dispersion relations are thus obtained as

$$E - V_0 = \frac{\imath(1 - \cos(\tilde{k}_1 \Delta x))}{5 + \cos(\tilde{k}_1 \Delta x)}, \quad (31)$$

and

$$E - V_{N_x} = \frac{\imath(1 - \cos(\tilde{k}_2 \Delta x))}{5 + \cos(\tilde{k}_2 \Delta x)}. \quad (32)$$

Taking Taylor's expansions of both right hand sides of (31) and (32), one finds out

$$E - V_0 = \frac{\hbar^2 \tilde{k}_1^2}{2m^*} + O(\Delta x^4), \quad E - V_{N_x} = \frac{\hbar^2 \tilde{k}_2^2}{2m^*} + O(\Delta x^4), \quad (33)$$

and subsequently,

$$\tilde{k}_1 = k_1 + O(\Delta x^4), \quad \tilde{k}_2 = k_2 + O(\Delta x^4). \quad (34)$$

Remark 1 Actually, (33) is generalized to

$$E - V_0 = \frac{\hbar^2 \tilde{k}_1^2}{2m^*} + O(\Delta x^p), \quad E - V_{N_x} = \frac{\hbar^2 \tilde{k}_2^2}{2m^*} + O(\Delta x^p), \quad (35)$$

when the discretization scheme applied to discretize (1) has p th order accuracy. This is because when we take Taylor's expansion of the related scheme, and substitute $\phi = e^{ik_1x}$, for instance, in the scheme, we have

$$\frac{\hbar^2 \tilde{k}_1^2}{2m^*} \phi + V_0 \phi + O(\Delta x^p) \phi = E \phi,$$

which indicates the first relation of (35).

Substituting (30) in (29), one gets discrete waves in opposite directions for $x \leq 0$ and $x \geq L$, respectively. Making linear combinations of the above discrete waves in opposite directions as described with (6), one obtains the approximation of the solution outside the device:

$$\psi_j = \begin{cases} R\alpha^{-j} + \alpha^j, & j \leq 0, \\ T\beta^j, & j \geq N_x, \end{cases} \quad (36)$$

where

$$\alpha \triangleq \alpha_+, \beta \triangleq \beta_+. \quad (37)$$

As a result of (36),

$$\psi_{-1} - \alpha\psi_0 = \alpha^{-1} - \alpha, \quad (38)$$

$$\psi_{N_x+1} - \beta\psi_{N_x} = 0 \quad (39)$$

are derived as an alternative discretization scheme of the TBCs, besides the C4TBCs.

Lemma 1 *Let $t > \max\{2(E - V_0), 2(E - V_{N_x})\}$ be fulfilled. (38) and (39) correspond fourth order discretizations of (7) and (8), respectively.*

Proof. Taking Taylor's expansion of $\psi(-\Delta x; k)$ at $x = 0$, one sees

$$\psi(-\Delta x; k) = \psi(0; k) - \psi'(0; k)\Delta x + \frac{\psi''(0; k)}{2!}\Delta x^2 - \frac{\psi^{(3)}(0; k)}{3!}\Delta x^3 + \frac{\psi^{(4)}(0; k)}{4!}\Delta x^4 + O(\Delta x^5). \quad (40)$$

According to (6), one gets

$$\psi^{(2n)}(0; k) = (ik_1)^{2n}\psi(0; k), \quad \psi^{(2n+1)}(0; k) = (ik_1)^{2n+1}(2 - \psi(0; k)). \quad (41)$$

Substituting (41) in (40), one further obtains

$$\begin{aligned} \psi(-\Delta x; k) &= -\psi'(0; k)\Delta x + \left[1 + \frac{(ik_1\Delta x)^2}{2!} + \frac{(ik_1\Delta x)^3}{3!} + \frac{(ik_1\Delta x)^4}{4!} \right] \psi(0; k) \\ &\quad + 2i \frac{(k_1\Delta x)^3}{3!} + O(\Delta x^5) \\ &= -[\psi'(0; k) + ik_1\psi(0; k) - 2ik_1]\Delta x + e^{ik_1\Delta x}\psi(0; k) \\ &\quad + e^{-ik_1\Delta x} - e^{ik_1\Delta x} + O(\Delta x^5). \end{aligned} \quad (42)$$

According to (34),

$$e^{ik_1\Delta x} = \alpha + O(\Delta x^5) \quad (43)$$

is natural, and

$$\psi'(0; k) + ik_1\psi(0; k) - 2ik_1 = -\frac{\psi_{-1} - \alpha\psi_0 - \alpha^{-1} + \alpha}{\Delta x} + O(\Delta x^4)$$

is thus obtained by substituting (43) in (42). Similarly,

$$\psi'(L; k) - ik_2\psi(L; k) = \frac{\psi_{N_x+1} - \beta\psi_{N_x}}{\Delta x} + O(\Delta x^4)$$

could be deduced similarly. \square

(38)-(39) is the so-called D4TBCs. According to **Lemma 1**, one arrives the first main result of this paper, i.e., **Theorem 1**.

Theorem 1 (24) equipped with the D4TBCs forms a globally fourth order discretization of the 1D Schrödinger problem. \square

At the end of this section, we point out the set of D4TBCs is a "good" candidate for discretizing the TBCs, not only because the accuracy order of the D4TBCs matches that of (24), more importantly, but also because the D4TBCs essentially avoid spurious oscillation in numerical solution when the potential vanishes. As an evidence and for comparison, we show norm of numerical wave function which solves (24) equipped with D4TBCs in **Fig. 1**, and one thing is obvious that oscillation in the numerical solution brought with the C4TBCs vanishes essentially when D4TBCs is used. This phenomenon is not accidental, since $\alpha^j = e^{i\tilde{k}(j\Delta x)}$ ($\tilde{k} = \tilde{k}_1 = \tilde{k}_2$) is the unique solution of (24) equipped with the D4TBCs when $V(x) \equiv 0$. Related conclusion and necessary proof are stated in **Theorem 2**.

As a preparation, which is also needed to prove **Theorem 2**, we introduce a discrete version of integral by parts law, i.e., **Lemma 2**.

Lemma 2 Assuming u and v are two grid functions defined on $\{x_i : -1 \leq i \leq N_x + 1\}$, one has

$$-\Delta x \sum_{i=0}^{N_x} (\delta_x^2 u_i) v_i = \Delta x \sum_{i=0}^{N_x+1} (\delta_x u_{i-\frac{1}{2}}) (\delta_x v_{i-\frac{1}{2}}) + (D_+ u_{-1}) v_{-1} - (D_- u_{N_x+1}) v_{N_x+1}, \quad (44)$$

where

$$\begin{aligned} \delta_x v_{i-\frac{1}{2}} &= \frac{1}{\Delta x} (v_i - v_{i-1}), \quad \delta_x^2 v_i = \frac{1}{\Delta x} (\delta_x v_{i+\frac{1}{2}} - \delta_x v_{i-\frac{1}{2}}), \\ D_+ v_i &= \frac{1}{\Delta x} (v_{i+1} - v_i), \quad D_- v_i = \frac{1}{\Delta x} (v_i - v_{i-1}). \end{aligned} \quad (45)$$

Proof. Clearly,

$$\begin{aligned}
-\Delta x \sum_{i=0}^{N_x} (\delta_x^2 u_i) v_i &= - \sum_{i=0}^{N_x} (\delta_x u_{i+\frac{1}{2}} - \delta_x u_{i-\frac{1}{2}}) v_i \\
&= \sum_{i=0}^{N_x} (\delta_x u_{i-\frac{1}{2}}) v_i - \sum_{i=1}^{N_x+1} (\delta_x u_{i-\frac{1}{2}}) v_{i-1} \\
&= \sum_{i=0}^{N_x+1} (\delta_x u_{i-\frac{1}{2}}) (v_i - v_{i-1}) + (\delta_x u_{-\frac{1}{2}}) v_{-1} - (\delta_x u_{N_x+\frac{1}{2}}) v_{N_x+1} \\
&= \Delta x \sum_{i=0}^{N_x+1} (\delta_x u_{i-\frac{1}{2}}) (\delta_x v_{i-\frac{1}{2}}) + (D_+ u_{-1}) v_{-1} - (D_- u_{N_x+1}) v_{N_x+1}.
\end{aligned}$$

□

Theorem 2 Let $t > \max \{2(E - V_0), 2(E - V_{N_x})\}$ be fulfilled. (24) equipped with the D4TBCs has unique solution for arbitrary $V(x)$.

Proof. Using (45), (24) and the D4TBCs are rewritten into

$$\begin{aligned}
\delta_x^2 \psi_j - \frac{\Delta x^2}{12} \delta_x^2 f_j &= f_j, \quad j = 0, 1, \dots, N_x, \\
\psi_{-1} - \alpha \psi_0 &= \alpha^{-1} - \alpha, \\
\psi_{N_x+1} - \beta \psi_{N_x} &= 0.
\end{aligned}$$

Obviously, uniqueness of the solution of (24) equipped with the D4TBCs is equivalent to

$$\delta_x^2 \psi_j - \frac{\Delta x^2}{12} \delta_x^2 f_j = f_j, \quad j = 0, 1, \dots, N_x, \quad (46)$$

$$\psi_{-1} - \alpha \psi_0 = 0, \quad (47)$$

$$\psi_{N_x+1} - \beta \psi_{N_x} = 0 \quad (48)$$

only has a trivial solution.

Multiplying (46) by $-\Delta x \psi_j^*$, where ψ_j^* denotes by the conjugate of ψ_j , and summing all equations with respect to j for $j \in \{0, 1, \dots, N_x\}$, we obtain

$$-\Delta x \sum_{j=0}^{N_x} (\delta_x^2 \psi_j) \psi_j^* + \frac{\Delta x^2}{12} \Delta x \sum_{j=0}^{N_x} (\delta_x^2 f_j) \psi_j^* = -\Delta x \sum_{j=0}^{N_x} f_j \psi_j^*. \quad (49)$$

Applying (44) to the two summations on the left of (49), one reorganizes the result as

$$A_1 = B_1 + C_1, \quad (50)$$

where

$$A_1 = \Delta x \sum_{j=0}^{N_x+1} (\delta_x \psi_{j-\frac{1}{2}}) (\delta_x \psi_{j-\frac{1}{2}}^*) + \Delta x \sum_{j=0}^{N_x} f_j \psi_j^*,$$

$$B_1 = \frac{\Delta x^2}{12} \Delta x \sum_{j=0}^{N_x+1} (\delta_x f_{j-\frac{1}{2}}) (\delta_x \psi_{j-\frac{1}{2}}^*),$$

$$C_1 = \frac{\Delta x^2}{12} [(D_+ f_{-1}) \psi_{-1}^* - (D_- f_{N_x+1}) \psi_{N_x+1}^*] - (D_+ \psi_{-1}) \psi_{-1}^* + (D_- \psi_{N_x+1}) \psi_{N_x+1}^*.$$

At the same time, we multiply both sides of (46) with $\frac{\Delta x^2}{12} (-\Delta x) f_j^*$, sum the yielded equations again with respect to j for $j \in \{0, 1, \dots, N_x\}$, and obtain

$$A_2 = B_2 + C_2, \quad (51)$$

where

$$A_2 = \frac{\Delta x^4}{144} \Delta x \sum_{j=0}^{N_x+1} (\delta_x f_{j-\frac{1}{2}}) (\delta_x f_{j-\frac{1}{2}}^*) - \frac{\Delta x^2}{12} \Delta x \sum_{j=0}^{N_x} f_j f_j^*,$$

$$B_2 = \frac{\Delta x^2}{12} \Delta x \sum_{j=0}^{N_x+1} (\delta_x \psi_{j-\frac{1}{2}}) (\delta_x f_{j-\frac{1}{2}}^*),$$

$$C_2 = \frac{\Delta x^2}{12} [(D_+ \psi_{-1}) f_{-1}^* - (D_- \psi_{N_x+1}) f_{N_x+1}^*] - \frac{\Delta x^4}{144} [(D_+ f_{-1}) f_{-1}^* - (D_- f_{N_x+1}) f_{N_x+1}^*].$$

Obviously, $A_1, A_2 \in \mathbb{R}$ and $B_1 = B_2^*$, which indicates

$$\text{Im}(C_1 + C_2) = 0. \quad (52)$$

By using (47)-(48), one concludes that (52) is equivalent to

$$\text{Im} (g_0 |\psi_{-1}|^2 \alpha^{-1} + g_{N_x} |\psi_{N_x+1}|^2 \beta^{-1}) = 0, \quad (53)$$

where

$$g_0 = \left(\frac{V_0 - E}{t} - 1 \right)^2 > 0, \quad g_{N_x} = \left(\frac{V_{N_x} - E}{t} - 1 \right)^2 > 0,$$

when $t > \max \{2(E - V_0), 2(E - V_{N_x})\}$. Recalling (37), one notices the imaginary parts of α and β have the same signs, thus

$$g_0 |\psi_{-1}|^2 = g_{N_x} |\psi_{N_x+1}|^2 = 0,$$

which implies

$$\psi_{-1} = \psi_{N_x+1} = 0. \quad (54)$$

Substituting (54) in (46)-(48), one finds out (46)-(48) admits a unique solution, which concludes the proof of the theorem. \square

3.3 The aDTBCs

Based on the discussions made in Sect. 3.2, pros and cons of the D4TBCs are quite clear. In one aspect, the accuracy order of the D4TBCs is consistent with the order of the interior scheme, which is delightful. More importantly, spurious oscillation in numerical solution is avoided, when $V(x) \equiv 0$. However, in the other aspect, an extra discrete dispersion relation is needed via solving an algebraic equation, with the order of the algebraic equation increased as the accuracy order of discretization scheme for the Schrödinger equation increases. At the same time, the dispersion relation brought numerical error, so does the D4TBCs consequently.

Actually, TBCs could be discretized without introducing discretization error, as long as $\psi(x; k)$ is analytic near physical boundaries. In the rest of this section, we always assume $\psi(x; k)$ be analytic near both physical boundaries. Taking (7) for instance, we use Taylor series with infinite terms to accurately express $\psi(-\Delta x; k)$:

$$\begin{aligned} \psi(-\Delta x; k) &= \psi(0; k) - \psi'(0; k)\Delta x + \frac{\psi''(0; k)}{2!}\Delta x^2 - \frac{\psi^{(3)}(0; k)}{3!}\Delta x^3 + \frac{\psi^{(4)}(0; k)}{4!}\Delta x^4 \\ &\quad - \frac{\psi^{(5)}(0; k)}{5!}\Delta x^5 + \dots \\ &= \left[1 + \frac{(ik_1\Delta x)^2}{2!} + \frac{(ik_1\Delta x)^3}{3!} + \frac{(ik_1\Delta x)^4}{4!} + \frac{(ik_1\Delta x)^5}{5!} + \dots \right] \psi(0; k) \\ &\quad - \Delta x \psi'(0; k) - 2i \left[-\frac{(k_1\Delta x)^3}{3!} + \frac{(k_1\Delta x)^5}{5!} - \dots \right] \\ &= -\Delta x [\psi'(0; k) + ik_1\psi(0; k) - 2ik_1] + e^{ik_1\Delta x} \psi(0; k) - 2i \sin(k_1\Delta x), \end{aligned}$$

where (41) is noticed. As a result, a discretization scheme for (7) without discretization error is yielded as

$$\psi_{-1} - e^{ik_1\Delta x} \psi_0 + 2i \sin(k_1\Delta x) = 0, \quad (55)$$

where k_1 and E satisfy the exact dispersion relation, i.e., $k_1 = \sqrt{\frac{2m^*(E-V_0)}{\hbar}}$. Similarly, the analytic discretization of (8) reads

$$\psi_{N_x+1} - e^{ik_2\Delta x} \psi_{N_x} = 0, \quad (56)$$

which does not introduce any discretization error, too. (55)-(56) is a specific example of the aDTBCs. Clearly, the overall accuracy order of (24) equipped with the aDTBCs totally depends on the appearance of the discretization scheme applied to discretize the Schrödinger equation. The result of the uniqueness of the solution of (24) equipped with the aDTBCs is provided in **Theorem 3**, where the proof is omitted due to its similarity with the proof of **Theorem 2**.

Theorem 3 *Let $t > \max\{2(E - V_0), 2(E - V_{N_x})\}$ be fulfilled. (24) equipped with the aDTBCs has unique solution for arbitrary $V(x)$. \square*

Table 1 Convergence orders of (24) equipped with the D4TBCs and the aDTBCs, respectively

BCs	$N_x = 200$	$N_x = 400$	$N_x = 800$
D4TBCs	4.00043	3.99986	4.00085
aDTBCs	4.00187	4.00137	4.00107

We make comparisons between the two discretization schemes: (24) equipped with the D4TBCs and the aDTBCs, respectively, by comparing their accuracy orders via solving the example studied in Sect. 3.2. Numerical results given in **Table 1** show that fourth order accuracy is globally achieved by (24) equipped with either one of the D4TBCs and the aDTBCs.

As depicted in **Fig. 1**, spurious oscillation exists in the numerical solution when $V \equiv 0$, too, when aDTBCs is applied. However, apparent reduction in amplitude of the spurious oscillation occurs, when the aDTBCs is compared to the C4TBCs. More importantly, it is not clear whether spurious oscillation still exists when $V(x) \neq 0$, by using any of boundary discretization schemes discussed in this paper, including the D4TBCs.

Thanks to the aDTBCs, one is able to improve the overall accuracy of the discretization scheme for the Schrödinger problem to arbitrarily high order. Applying (18) to discretize (1) at grid points x_i , $i = 0, 1, \dots, N_x$, one finds out it is necessary to express $(\psi_{xx})_i$ and ψ_i for $i < 0$ and $i > N_x$ with interior or with boundary nodal values of ψ to close the equations. Noticing ψ solves (1) outside the device with (4) satisfied, i.e., $(\psi_{xx})_{i < 0 (i > N_x)} = \frac{2m^*}{\hbar^2}(V_{i < 0 (i > N_x)} - E)\psi$, where $V_{i < 0} = V_0$ and $V_{i > N_x} = V_{N_x}$, one observes unknowns outside the device region really needed to be expressed are $\{\psi_j, j = -1, \dots, -L\}$ and $\{\psi_{N_x+j}, j = 1, \dots, L\}$, with $L = \max\{l, s\}$. Similar to the way that adopted in deriving (55), we consider Taylor series of $\psi(-j\Delta x; k)$, $j = 1, 2, \dots, L$, with infinite terms, and deduce two sets of accurate discretizations of the TBCs, which read

$$\psi_{-j} - e^{ik_1(j\Delta x)}\psi_0 + 2i \sin(k_1(j\Delta x)) = 0, \quad j = 1, 2, \dots, L, \quad (57)$$

and

$$\psi_{N_x+j} - e^{ik_2(j\Delta x)}\psi_{N_x} = 0, \quad j = 1, 2, \dots, L. \quad (58)$$

(57) and (58) stand for a general framework of the aDTBCs, with which the overall accuracy of discretization for the 1D Schrödinger problem could be improved to arbitrarily high levels.

However, DTBCs consistent with arbitrarily high order interior discretization are essentially impossible to be deduced for $L \geq 3$. The reason for the above assertion is that to derive the required DTBCs, one needs to analytically solve a high order (at least 6th order) algebraic equation, in order to obtain the corresponding discrete dispersion relations, which is theoretically impossible. Therefore, the aDTBCs could be used as an alternative choice besides DTBCs, when $V \neq 0$ in simulating realistic devices or high order schemes are desired.

4 The iterative scheme for solving the Schrödinger-Poisson problem

Firstly, we instantiate (14) with the Poisson problem. Applying (21) to discretize (2) at interior grid points, one obtains

$$\lambda(V_s)_{i-1} - f_{i-1} - [2\lambda(V_s)_i + 10f_i] + \lambda(V_s)_{i+1} - f_{i+1} = 0, \dots, i = 1, \dots, N_x - 1, \quad (59)$$

where $(V_s)_i$ denotes the approximation of $V_s(x_i)$, and

$$f_i = \frac{q_e^2}{\epsilon} (N_d(x_i) - n_i), \quad (60)$$

where n_i is the approximation of $n(x)$ at x_i . According to (11), the density of electron is defined as an integral on the real line, thus truncation of the integral is necessary in numerical calculations. For E_F used in all of the numerical experiments, one finds out $F(E_F - E)$, which is given by (10), is less than 10^{-10} when $E > 0.8$ (eV). Therefore, we truncate the integral range into $[0, 0.8]$ (eV) and calculate n_i via the adaptive Simpson quadrature routine[13].

One further applies (23) to discretize (3) at x_0 and x_{N_x} , respectively, and obtains the corresponding discretization schemes in the form of

$$\frac{(V_s)_1 - (V_s)_{-1}}{2\Delta x} - \frac{\Delta x}{12} (f_1 - f_{-1}) = 0, \quad (61)$$

and

$$\frac{(V_s)_{N_x+1} - (V_s)_{N_x-1}}{2\Delta x} - \frac{\Delta x}{12} (f_{N_x+1} - f_{N_x-1}) = 0. \quad (62)$$

Applying (59) to discretize (2) at x_0 and x_{N_x} , and combining the results with (61) and (62) respectively, one closes (59) with fourth order discretization of (3), i.e.,

$$\begin{aligned} -2\lambda(V_s)_0 + 2\lambda(V_s)_1 &= -f_{-1} + 10f_0 + 3f_1, \\ 2\lambda(V_s)_{N_x-1} - 2\lambda(V_s)_{N_x} &= 3f_{N_x-1} + 10f_{N_x} - f_{N_x+1}. \end{aligned} \quad (63)$$

where f_{-1} and f_{N_x+1} are defined according to (60), and approximated with the adaptive Simpson quadrature mentioned previously, where ψ_{-1} and ψ_{N_x+1} involved in the integrals are determined through the D4TBCs or the aDTBCs. As a result, a globally fourth order discretization of the 1D Schrödinger-Poisson problem is proposed by equipping (24) with the D4TBCs or the aDTBCs, and coupling (59) equipped with (63). For the convenience of subsequent discussion, we name (24) with the D4TBCs and the aDTBCs as the DS1 and the DS2, respectively, and the whole 1D discrete Schrödinger-Poisson system involving the D4TBCs and the aDTBCs as the DSP1 and the DSP2, respectively.

The details of the simulation process are given in **Algorithm 1**.

Algorithm 1

- 1 Make an initial guess about $V_s(x)$. For example, the setup is $V_s(x) \equiv 0$ for RTD simulation.
- 2 For any given energy E , solve (24) equipped with either the D4TBCs or the aDTBCs to obtain corresponding discrete wave functions.

3 If $V(x)$ is known *a priori*, then terminate the iteration. Otherwise, calculate n_i , $i = -1, 0, \dots, N_x + 1$, via the adaptive Simpson quadrature routine, where discrete wave functions corresponding to plenty of sampling values of E should be solved repeatedly according to step 2. Then apply Newton-Raphson iteration [17, 10] to solve (59) equipped with (63). The criterion to end this Newton-Raphson iteration is

$$\|(\mathbf{V}_s)^{(p+1)} - (\mathbf{V}_s)^{(p)}\|_{L^\infty} \leq 10^{-10}, \quad (64)$$

where p denotes the iteration step.

4 Repeat step 2 and step 3 till the numerical solution of the Schrödinger-Poisson problem converges, where the criterion for the convergence is the same as that used in the 3rd step, where p is the iteration step of the whole iteration.

5 Numerical experiments

In this section, we use several examples, including a short $n^{++} - n^+ - n^{++}$ resistor and two RTDs, to validate theoretical accuracy orders of the discretizations, and the ability of **Algorithm 1** in simulating quantum devices.

5.1 A one dimensional $n^{++} - n^+ - n^{++}$ resistor

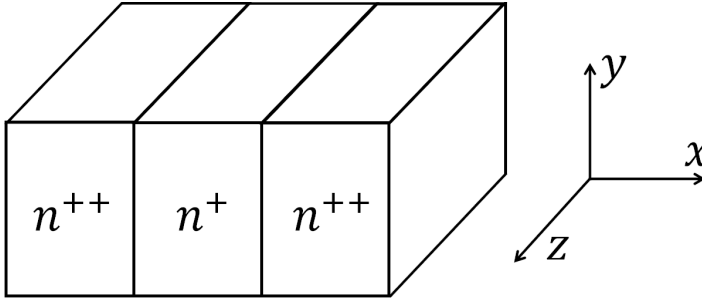


Fig. 2 Skeleton of a three dimensional $n^{++} - n^+ - n^{++}$ resistor, where the transport of electrons in the x -direction is of concern

In **Fig. 2**, the skeleton of a short three dimensional $n^{++} - n^+ - n^{++}$ resistor is shown. We further assume all physical quantities involved are homogeneous in both the y -direction and the z -direction, thus the problem could be simplified as simulation of a one dimensional resistor, where the appearance of electrons in the x -direction is of concern. Parameters are set as that used in [5], which read: $m = 0.25m_0$, where $m_0 = 9.1 \times 10^{-31}$ (Kg), $\varepsilon = 10\varepsilon_0$, where $\varepsilon_0 = 8.85 \times 10^{-12}$ (F m⁻¹), $T_L = 300$ (K), and $E_F = 0.318$ (eV). The device is 30 (nm) long in total and discretized with a uniform

grid with 100 grid points. $V_b \equiv 0$ and the doping profile reads

$$N_d(x) = \begin{cases} 10^{20} \text{ cm}^{-3}, & x \in [0, 4.5] \cup [25.5, 30](\text{nm}), \\ 5 \times 10^{19} \text{ cm}^{-3}, & x \in (4.5, 25.5)(\text{nm}). \end{cases} \quad (65)$$

The simulation is carried out following **Algorithm 1**, where the numerical results are in **Fig. 3**, **Fig. 4**, **Fig. 5**, and **Table 2**. Appearance of **Algorithm 1** in simulating the 1D $n^{++} - n^+ - n^{++}$ resistor is studied, by taking results obtained via solving the problem yielded by applying the second order NEGF method[5] as benchmarks. Numerical results about the potential functions and densities of electrons are shown in **Fig. 3** with $V_{ds} = 0$ (V) and $V_{ds} = 0.25$ (V), respectively. Vividly, curves simulated following **Algorithm 1** match that solved with the second order NEGF method.

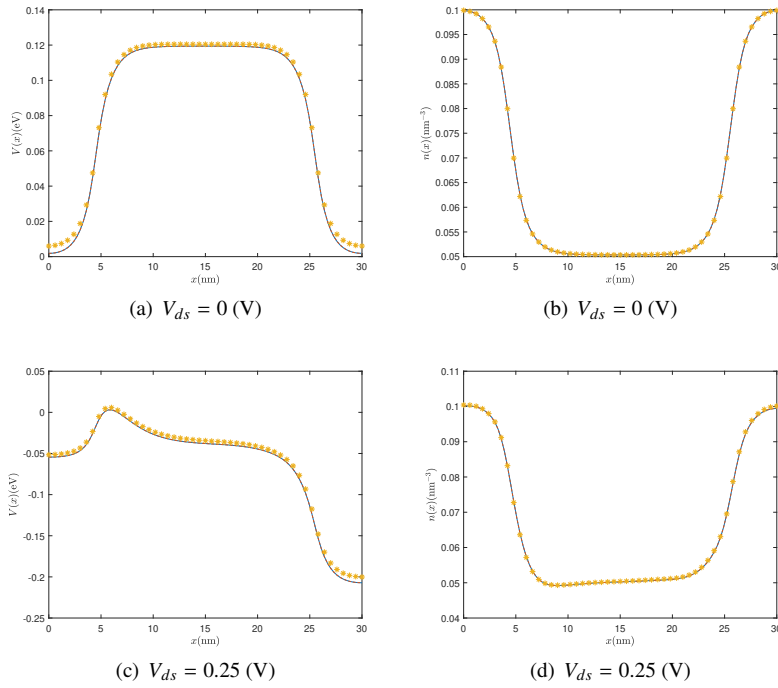


Fig. 3 Numerical results about the potential functions $V(x)$ (on the left) and density functions $n(x)$ (on the right) simulated with two samplings of V_{ds} , i.e., 0 (V) and 0.25 (V), respectively. The DSP1(in blue solid line) and the DSP2(in red dash line) are both considered, for both values of V_{ds} , separately. Corresponding results(in star) solved with the second order NEGF method are shown as benchmarks

Table 2 Convergence orders of DSP1 and DSP2

Method	$N_x = 100$	$N_x = 200$	$N_x = 400$	$N_x = 800$
DSP1	4.0475	3.9906	4.0073	4.0815
DSP2	4.0178	3.9997	4.0052	4.0859

In order to examine the theoretical accuracy orders of the DSP1 and the DSP2, respectively, we smooth the doping density function with

$$\phi(x) = \frac{5e^{5x}}{(1 + e^{5x})^2}, \quad (66)$$

and $V_{ds} = 0$ (V) during the simulation. We define error vector $\delta V_{\Delta x}$ as the absolute error of $V_{\Delta x}$ with respect to V^* , where $V_{\Delta x}$ denotes the potential function solved on a grid with grid space Δx , and V^* is the projection of $V_{L/1600}$ in the space where $V_{\Delta x}$ lies in. The error function of the numerical solution is defined as

$$E_{\Delta x} = \max \delta V_{\Delta x}, \quad (67)$$

and the accuracy order is estimated by calculating $\log_2 \left(\frac{E_{\Delta x}}{E_{\Delta x/2}} \right)$ with gradually halved Δx . Numerical results about the convergence behavior and convergence orders of DSP1 and DSP2 are separately shown in **Fig. 4** and **Table 2**, which both indicate good convergence of them.

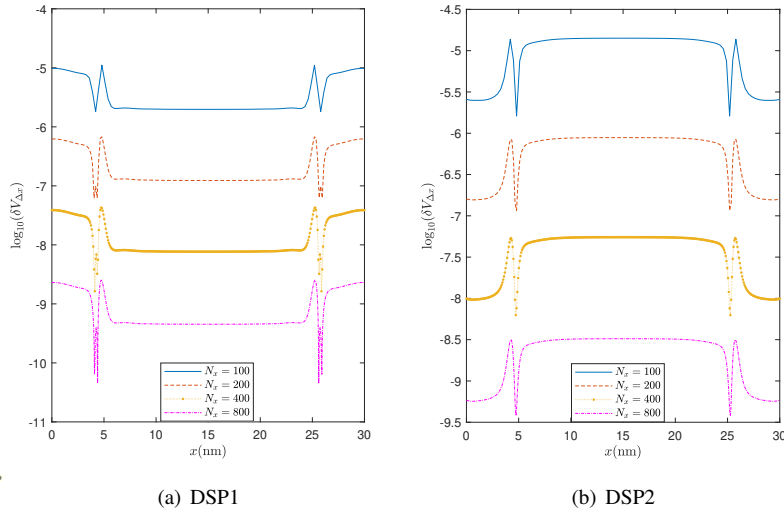


Fig. 4 Tendency of $\log_{10}(\delta V_{\Delta x})$ with respect to decreasing Δx , where the DSP1(a) and the DSP2(b) are considered separately

At last, we show the I-V characteristic curves of the 1D $n^{++} - n^+ - n^{++}$ resistor in **Fig. 5**, which are simulated with **Algorithm 1**, by considering the DSP1 and the DSP2 in the algorithm, respectively. Constant resistance values are observed in both simulations, which is a characteristic of classic devices. Furthermore, convergence of I-V characteristic curves with respect to decreasing grid sizes indicates convergence of both the DSP1 and the DSP2.

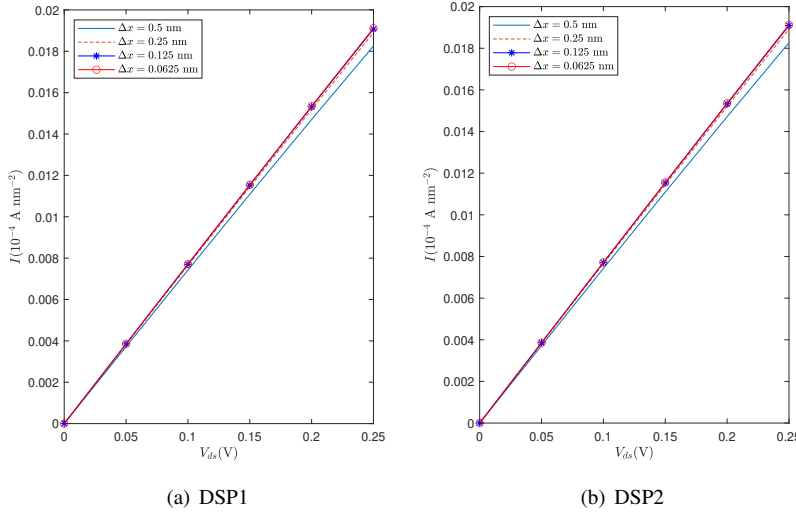


Fig. 5 I-V characteristic curves of the 1D resistor simulated with decreasing Δx , where the DSP1(a) and the DSP2(b) are considered, respectively

5.2 RTDs

In this section, we study the RTD device with the same structure as what was studied in [15]. The skeleton of the RTD is shown in **Fig. 6**. The RTD device is 135(nm) long in total, and is doped according to

$$N_d(x) = \begin{cases} 10^{18} \text{ cm}^{-3}, & x \in [0, 50] \cup [85, 135](\text{nm}), \\ 5 \times 10^{15} \text{ cm}^{-3}, & x \in (50, 85)(\text{nm}), \end{cases}$$

which is smoothed out in all of the simulations. The rest of parameters read: $m = 0.067m_0$, where $m_0 = 9.1 \times 10^{-31}$ (Kg), $\varepsilon = 11.44\varepsilon_0$, where $\varepsilon_0 = 8.85 \times 10^{-12}$ (F m⁻¹), and $E_F = 0.0427$ (eV).

A double barrier potential with the profile of

$$V_b(x) = \begin{cases} V_0, & x \in [60, 65] \cup [70, 75](\text{nm}), \\ 0, & x \in [0, 60) \cup (65, 70) \cup (75, 135](\text{nm}), \end{cases}$$

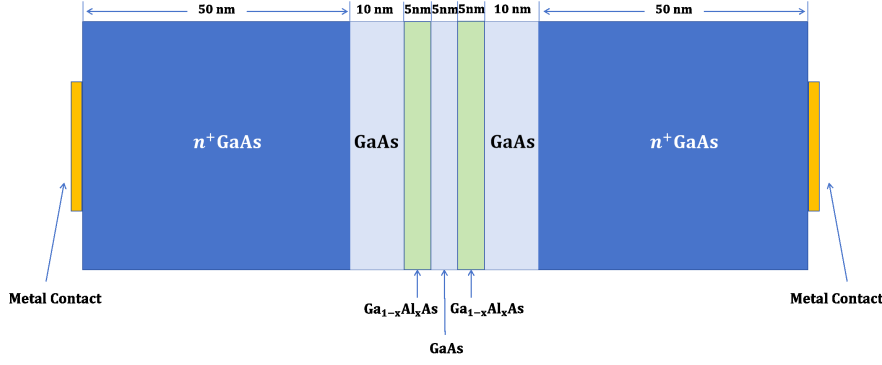


Fig. 6 Skeleton of the RTD

is contained within the device, where V_0 is a prescribed height of the double-barrier and is set to 0.3 (eV) in the following experiments. The other component of the potential function $V(x)$, i.e., $V_s(x)$ is either set in advance (RTD A), or studied with a Poisson equation self-consistently (RTD B).

5.2.1 RTD A

In this example, $V_s(x)$ is a continuous function set in advance, which reads

$$V_s(x) = \begin{cases} 0, & x \in [0, 50](\text{nm}), \\ -q_e V_{ds} \frac{x-50}{35}, & x \in (50, 85)(\text{nm}), \\ -q_e V_{ds}, & x \in [85, 135](\text{nm}). \end{cases} \quad (68)$$

We smooth $V(x)$ with (66) in order to conduct accuracy order tests. In this example, V_{ds} is increased from zero, and by $\Delta V_{ds} = 0.02$ (V) each time. We simulate the I-V characteristic curve of RTD A with **Algorithm 1**, and consider the D4TBCs and the aDTBCs in applying the algorithm. Results about the I-V characteristic I-V curve are shown in **Fig. 7**, for both discrete boundary conditions, respectively. Obviously, current densities solved with both of the D4TBCs and the aDTBCs, show sharp peaks with similar heights around 0.18 (V). Furthermore, all of these I-V characteristic curves show negative resistance, which corresponds to one of the most typical characteristics of quantum devices. To test the convergence of both the DS1 and the DS2, we use gradually refined mesh grids to simulate I-V characteristic curves, where the finest grid space is 0.5 (nm). Clearly, fast convergence of I-V curves is observed in both simulations with the DS1 and the DS2, respectively.

5.2.2 RTD B

Unlike RTD A studied in Sect. 5.2.1, $V_s(x)$ exerted to RTD B is updated simultaneously with $\psi(x; k)$, via solving (59) equipped with (63) self-consistently, according to **Algorithm 1**. The temperature of lattice is set to 300 (K), $\Delta V_{ds} = 0.02$ (V) and

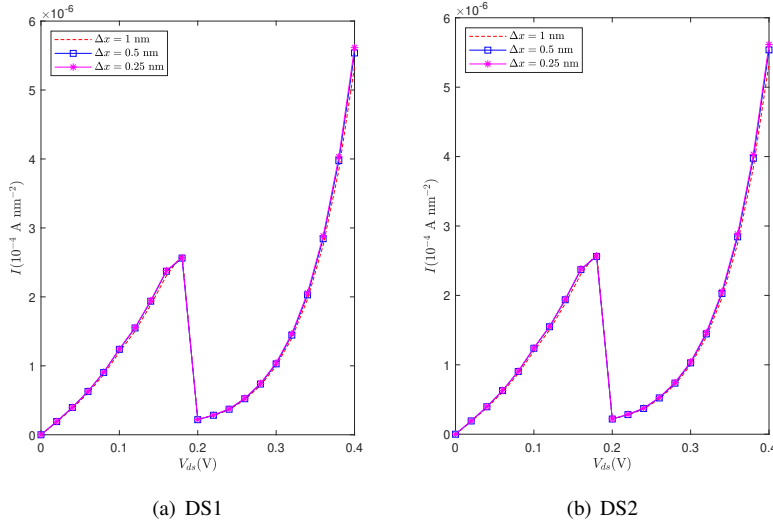


Fig. 7 I-V characteristic curves of RTD A with respect to DS1(a) and DS2(b), respectively, where gradually refined mesh grids are used

$\Delta x = 0.5$ (nm). I-V characteristic curves corresponding to the DSP1 and the DSP2, are shown in **Fig. 8**, respectively. Obviously, the two I-V characteristic curves corresponding to the DSP1 and the DSP2 match very well, and they both show peak values around $V_{ds} = 0.26$ (V). In addition, the negative resistance phenomenon is observed from both curves.

In **Fig. 9**, **Fig. 10** and **Fig. 11**, we show stable electron densities and potential functions at three different values of V_{ds} , which are 0.1 (V), 0.26 (V) and 0.28 (V), respectively. One observes that there are more electrons within the quantum well at 0.26 (V), than that at 0.1 (V) and 0.28 (V), both. This phenomenon is expected, since the current density takes its peak value at 0.26 (V) as is shown in **Fig. 8**.

At last, we show transmission coefficient of the device, where simulation results obtained with the DSP1 and the DSP2 are shown separately in **Fig. 12**. On the one hand, curves simulated with the DSP1 and the DSP2 are very similar, which indicates the accuracy of both models. On the other hand, the transmission coefficient exhibits a series of resonant peaks which could be explained according to [20]. When E is close to the resonant levels of the well, the wave proceeds through the first barrier into the well, while simultaneously a wave of equal intensity flows out of the well on the other side through the other barrier. In addition, peaks of the transmission coefficient shift towards the lower energy region, and the peak value decreases when V_{ds} increases. In fact, the transmission coefficient can be approximated by a Lorentzian-type function

$$T(E, V_{ds}) = \frac{\sqrt{1 - \left(\frac{q_e V_{ds}}{2E_n}\right)^2}}{1 + \left(\frac{2(E - E_n)}{\Delta E}\right)^2},$$

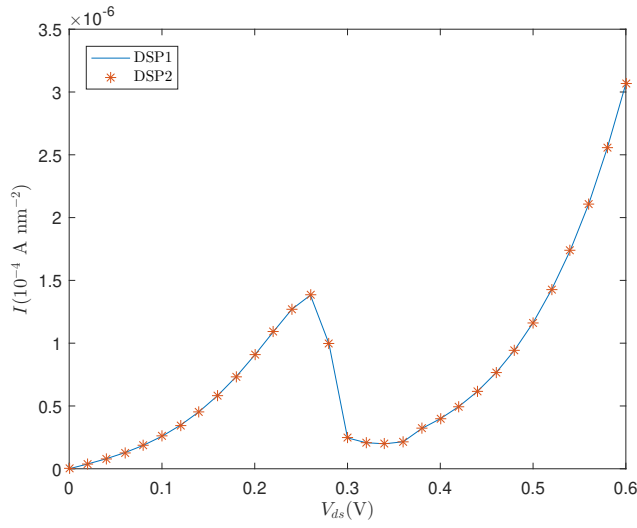


Fig. 8 Simulation results about the I-V characteristic curve of RTD B, where the DSP1 and the DSP2 are solved respectively

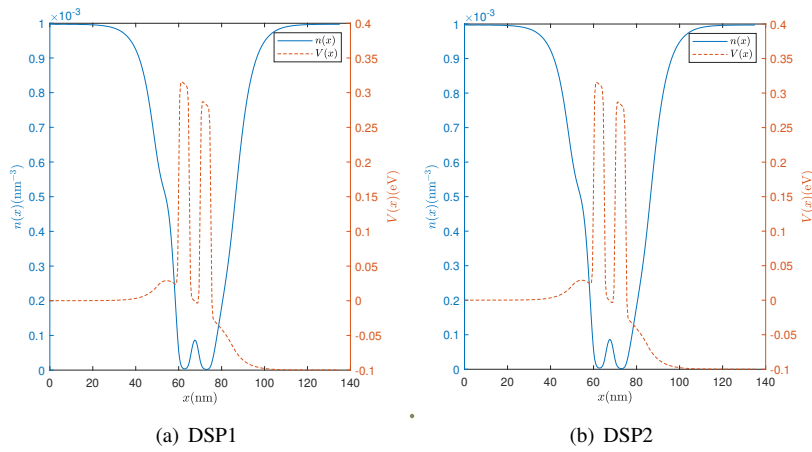


Fig. 9 Electron density $n(x)$ and total potential $V(x)$ simulated with $V_{ds} = 0.1$ (V)

where E_n is the energy of the resonant level and ΔE denotes the total broadening of the energy level. Since resonance occurs when $E = E_n - \frac{q_e V_{ds}}{2}$, the resonant peaks shift when V_{ds} changes.

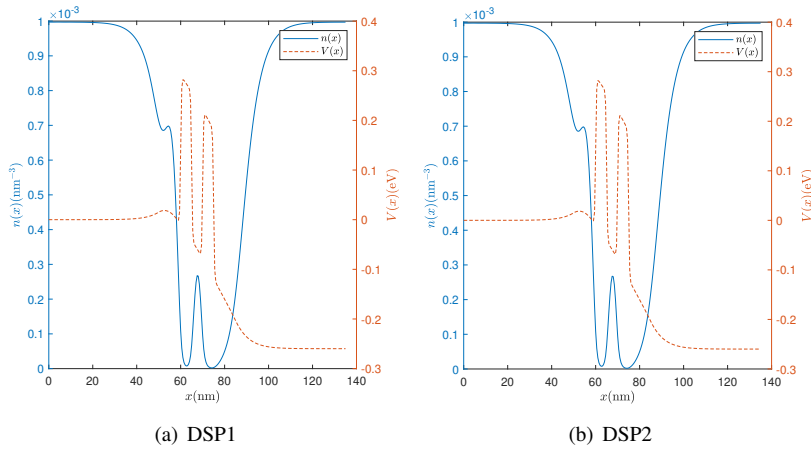


Fig. 10 Electron density $n(x)$ and total potential $V(x)$ simulated with $V_{ds} = 0.26$ (V)

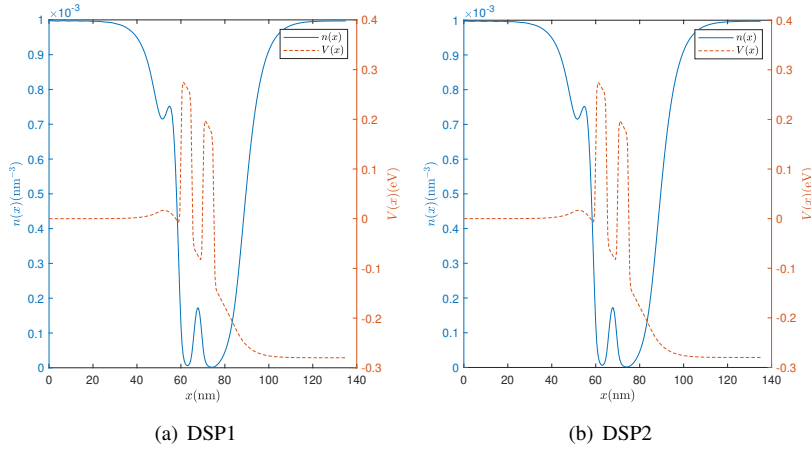


Fig. 11 Electron density $n(x)$ and total potential $V(x)$ simulated with $V_{ds} = 0.28$ (V)

6 Conclusion

In this paper, we introduce two optimal discretization schemes for the TBCs of the 1D Schrödinger equation, i.e., the D4TBCs and the aDTBCs. The D4TBCs could essentially avoid spurious oscillation in numerical solutions when the potential vanishes, and possesses the same accuracy order with the discretization scheme applied to discretize the 1D Schrödinger equation. However, the D4TBCs can not be generalized to arbitrarily high order since an algebraic equation should be solved explicitly, which is impossible because the order of the algebraic equation increases as the accu-

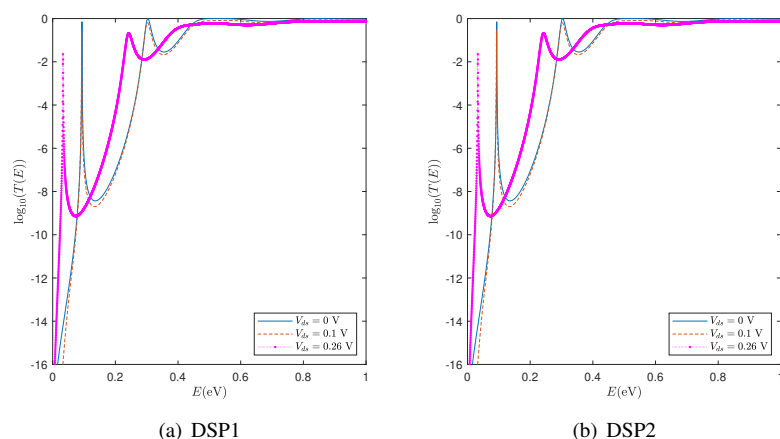


Fig. 12 Transmission coefficient in logarithmic scale for three different biases

racy order increases. To overcome that, we further propose a framework of aDTBCs, which is accurate in discretizing the TBCs, and could easily be generalized to arbitrarily high order. Involving the D4TBCs and the aDTBCs, two globally fourth order compact finite difference schemes are introduced for discretizing the 1D Schrödinger-Poisson problem, and an algorithm is proposed to simulate semiconductor devices. Numerical simulations are carried out for a classic resistor and two RTDs, and simulation results successfully verify the accuracy orders of both schemes and show characteristics of these devices.

Declarations

Funding This work was supported in part by the NSFC (Grant Numbers: 12171035, 12131001) and the Natural Science Foundation of Guangdong Province of China (Grant Number: 2024A1515010356).

Data Availability The datasets generated during and/or analysed during the current study are available in the figshare repository, https://figshare.com/articles/dataset/1DSchrodinger_TBC/25765377.

Conflict of interest The authors declare that they have no known competing financial interests or personal relationships that could have appeared to influence the work reported in this paper.

References

1. Anton Arnold. Mathematical concepts of open quantum boundary conditions. *Transp. Theory Stat. Phys.*, 30:561–584, 2001. <https://doi.org/10.1081/TT-100105939>.
2. Naoufel Ben Abdallah, Pierre Degond, and Peter A Markowich. On a one-dimensional Schrödinger-Poisson scattering model. *Z. angew. Math. Phys.*, 48:135–155, 1997. <https://doi.org/10.1007/pl00001463>.

3. L. L. Chang, L. Esaki, and R. Tsu. Resonant tunneling in semiconductor double barriers. *Appl. Phys. Lett.*, 24:593–595, 1974. <https://doi.org/10.1063/1.1655067>.
4. S. Datta, F. Assad, and M.S. Lundstrom. The silicon MOSFET from a transmission viewpoint. *Superlattices Microstruct.*, 23:771–780, 1998. <https://doi.org/10.1006/spmi.1997.0563>.
5. Supriyo Datta. Nanoscale device modeling: the Green's function method. *Superlattices Microstruct.*, 28:253–278, 2000. <https://doi.org/10.1006/spmi.2000.0920>.
6. Supriyo Datta and Michael J McLennan. Quantum transport in ultrasmall electronic devices. *Rep. Prog. Phys.*, 53:1003, 1990. <https://doi.org/10.1088/0034-4885/53/8/001>.
7. William R. Frensley. Wigner-function model of a resonant-tunneling semiconductor device. *Phys. Rev. B*, 36:1570–1580, 1987. <https://doi.org/10.1103/PhysRevB.36.1570>.
8. K. L. Jensen and F. A. Buot. Numerical simulation of intrinsic bistability and high-frequency current oscillations in resonant tunneling structures. *Phys. Rev. Lett.*, 66:1078–1081, 1991. <https://doi.org/10.1103/PhysRevLett.66.1078>.
9. Haiyan Jiang, Sihong Shao, Wei Cai, and Pingwen Zhang. Boundary treatments in non-equilibrium Green's function (NEGF) methods for quantum transport in nano-MOSFETs. *J. Comput. Phys.*, 227:6553–6573, 2008. <https://doi.org/10.1016/j.jcp.2008.03.018>.
10. Roger Lake, Gerhard Klimeck, R. Chris Bowen, and Dejan Jovanovic. Single and multiband modeling of quantum electron transport through layered semiconductor devices. *J. Appl. Phys.*, 81:7845–7869, 1997. <https://doi.org/10.1063/1.365394>.
11. Sanjiva K. Lele. Compact finite difference schemes with spectral-like resolution. *J. Comput. Phys.*, 103:16–42, 1992. [https://doi.org/10.1016/0021-9991\(92\)90324-R](https://doi.org/10.1016/0021-9991(92)90324-R).
12. Xuliang Liu, Shuhai Zhang, Hanxin Zhang, and Chi-Wang Shu. A new class of central compact schemes with spectral-like resolution I: Linear schemes. *J. Comput. Phys.*, 248:235–256, 2013. <https://doi.org/10.1016/j.jcp.2013.04.014>.
13. J. N. Lyness. Notes on the adaptive Simpson quadrature routine. *J. Assoc. Comput. Mach.*, 16:483–495, 1969. <https://doi.org/10.1145/321526.321537>.
14. Jan-Frederik Mennemann, Ansgar Jünger, and Hans Kosina. Transient Schrödinger–Poisson simulations of a high-frequency resonant tunneling diode oscillator. *J. Comput. Phys.*, 239:187–205, 2013. <https://doi.org/10.1016/j.jcp.2012.12.009>.
15. Olivier Pinaud. Transient simulations of a resonant tunneling diode. *J. Appl. Phys.*, 92:1987–1994, 2002. <https://doi.org/10.1063/1.1494127>.
16. Farhan Rana, Sandip Tiwari, and D. A. Buchanan. Self-consistent modeling of accumulation layers and tunneling currents through very thin oxides. *Appl. Phys. Lett.*, 69:1104–1106, 1996. <https://doi.org/10.1063/1.117072>.
17. Zhibin Ren, R. Venugopal, S. Goasguen, S. Datta, and M.S. Lundstrom. nanoMOS 2.5: A two-dimensional simulator for quantum transport in double-gate MOSFETs. *IEEE Trans. Electron Devices*, 50:1914–1925, 2003. <https://doi.org/10.1109/TED.2003.816524>.
18. R. Tsu and L. Esaki. Tunneling in a finite superlattice. *Appl. Phys. Lett.*, 22:562–564, 1973. <https://doi.org/10.1063/1.1654509>.
19. Masahiro Tsuchiya, Hiroyuki Sakaki, and Junji Yoshino. Room temperature observation of differential negative resistance in an AlAs/GaAs/AlAs resonant tunneling diode. *Jpn. J. Appl. Phys.*, 24:L466, 1985. <https://doi.org/10.1143/JJAP.24.L466>.
20. Sneha Lata Yadav and Hakim Najeeb-Ud-Din. A simple analytical model for the resonant tunneling diode based on the transmission peak and scattering effect. *J. Comput. Electron.*, 19:1061–1067, 2020. <https://doi.org/10.1007/s10825-020-01531-4>.